energies

MDPI

Article

Analyses of Interpolant Ion Effects on Smart Water Core Flooding in Carbonate

Ladislane dos Santos Bastos [1], Igor Emanuel da Silva Lins [1], Gloria Meyberg Nunes Costa [1] and Silvio Alexandre Beisl Vieira de Melo [1,2,*]

[1] Programa de Pós-Graduação em Engenharia Industrial, Escola Politécnica, Universidade Federal da Bahia, Rua Aristides Novis, 2, Federação, Salvador 40210-630, Brazil
[2] Centro Interdisciplinar em Energia e Ambiente, Campus Universitário da Federação/Ondina, Universidade Federal da Bahia, Rua Barão de Jeremoabo, S/N, Ondina, Salvador 40170-115, Brazil
* Correspondence: sabvm@ufba.br

Abstract: Smart water flooding (SWF) is a promising enhanced oil recovery (EOR) technique due to its economic advantages. For this process, wettability alteration is the most accepted controlling effect that leads to increased recovery factors (RFs). The main objective of this work is to investigate how the relative permeability curves' interpolant affects the SWF mechanisms' assessment. Wettability alteration is described by shifting these curves in simulations. Numerical simulations of core flooding tests are applied to carbonate at 114.4 °C. A comparison of oil recovery factor (RF), pH and effluent composition is performed for different injection approaches. Mg^{2+} and SO_4^{2-} are the interpolant ions and the salinity levels range from 30 to 1 kppm. A simulation of 24 scenarios, 12 for each type of interpolant, is presented. Results show that RF changes significantly, due to salinity and composition, for each interpolant. This has a relevant influence on the interpolant. The greater the dilution, the smaller the effect of the interpolant and brine composition on the recovery estimates. When considering SO_4^{2-} as an interpolant, the trend is that divalent rich brine (DV) has a higher recovery factor. In contrast, when Mg^{2+} is the interpolant, DV tends to have a lower recovery. The analysis of ionic exchange and pH variation corroborate the wettability alteration behavior. A pH increase was observed in all scenarios, regardless of the salinity, ion composition or interpolant variation. Also, monitoring the CH_3COO-X reduction and SO_4-X_2 increase equivalent fractions indicated the ion exchange mechanism as being well represented in all simulations. In addition, the results emphasize that even at very low concentrations, SO_4^{2-} plays a fundamental role in initiating the ion exchange process that culminates in the wettability alteration as a consequence of smart water injection.

Keywords: smart water flooding; interpolants; carbonate; simulation

check for updates

Citation: Bastos, L.d.S.; Lins, I.E.d.S.; Costa, G.M.N.; Vieira de Melo, S.A.B. Analyses of Interpolant Ion Effects on Smart Water Core Flooding in Carbonate. *Energies* **2023**, *16*, 446. https://doi.org/10.3390/en16010446

Academic Editors: Md Motiur Rahman, Mohamed R. Haroun and Abdulrazag Zekri

Received: 12 November 2022
Revised: 12 December 2022
Accepted: 21 December 2022
Published: 30 December 2022

Copyright: © 2022 by the authors. Licensee MDPI, Basel, Switzerland. This article is an open access article distributed under the terms and conditions of the Creative Commons Attribution (CC BY) license (https://creativecommons.org/licenses/by/4.0/).

1. Introduction

Waterflooding is the most commonly used method in oil fields for additional oil recovery after reservoir depletion. This method consists of maintaining or restoring the reservoir pressure and displacing the oil to the producing well by this driving force. It is a well-established, low-cost, and environmentally friendly method. However, high values of residual oil saturation are observed [1,2]. Carbonate rocks represent a large portion of the world's oil reservoirs (estimated at 60%), including 80% of the Middle East oil-bearing formations that accounts for approximately 75% of global oil production, so it has gained the attention of many researchers [3,4]. However, some challenges have been identified when analyzing oil recovery in this type of mineral: complex heterogeneity, fractured reservoirs, low recovery compared to sandstone results, and a tendency to a neutral or oil-wet state [3–6]. Especially in carbonate rocks, waterflooding has not been a recommended recovery method, as it is necessary to overcome high capillary forces to recover a low volume of oil [1,6]. Xu et al. (2020) [4] highlights the importance of further research to develop and understand EOR methods in carbonate reservoirs.

Among the methods recently investigated for these systems, smart water flooding (SWF) is easily implemented because it is based on waterflooding facilities and does not require adding any expensive chemicals [7]. This enhanced oil recovery method uses water with optimized composition, i.e., both the salinity and ionic composition of injected water (typically seawater or produced water) are modified to improve the production indices. Other names have also been used for this technique, such as ion-tuned or engineered water flooding. Despite being a nomenclature treated separately by some authors, low salinity water is also termed smart water based only on the reduction of salt concentration. Promising results from smart water flooding have been observed in laboratory tests and field applications. Although smart water injection has already been successfully applied in sandstone reservoirs, field tests in carbonate reports are limited. Yousef et al. (2011) [8], Yousef et al. (2011) [9], Yousef et al. (2012) [10] and Rassenfoss (2016) [11], highlight the efforts of the Saudi Arabian Oil Company research center to investigate this type of process applied to carbonate reservoirs. However, the applicability as a recovery method in reservoirs is still not widely observed, which is justified by Hao et al. (2019) [12] due to the existing gaps related to understanding the SWF mechanisms in this type of mineralogy. There is still much discussion about the exact mechanisms that lead to improving recovery, especially when carbonate rocks are involved [2,13–16]. Egbe et al. (2021) [3] and Awolayo and Sarma (2017) [17] highlight that the carbonate's heterogeneous nature makes it more difficult to understand the oil recovery mechanisms. It occurs because there is high bonding energy to carbonate rocks and oil components in reservoirs predominantly composed of calcite, dolomite and magnesite.

Wettability alteration from oil-wet to water-wet is the main effect on carbonates observed. It has been widely accepted due to different mechanisms: multiple ion exchanges, mineral dissolution leading to a pH increase and fines migration, electrical double layer expansion, interfacial tension reduction, and microdispersions formation [3]. In turn, the injection of water with a projected composition, can disturb the established chemical equilibrium between oil, rock and brine in the porous medium [15,18,19]. In this context, experimental investigation has also demonstrated the divalent ions Ca^{2+}, Mg^{2+} and $SO_4{}^{2-}$ are potential determining ions (PDI) to promote oil detachment from the rock surface and alter wettability and oil recovery due to multiple ion exchanges [2,20–22]. It is proposed that sulfate present in the injected water tends to adsorb on the carbonate surface, which is positively charged in the presence of the formation water. Due to this adsorption of negative ions, calcium cations can approximate the rock and form a complex with the carboxylic acids in the oil, releasing them from the mineral. And at high temperatures (>90 °C), magnesium cations can replace Ca^{2+} [23–25].

As experimental investigations are time-consuming and expensive, simulation of recovery methods has been an important tool for evaluating new techniques before implementation on a field scale. For modeling EOR methods, oil recovery and displacement mechanisms in the porous medium must be described through numerical formulations. For instance, transport phenomena laws, such as Darcy's law, material and energy balance equations, chemical reactions, equations of state, and other equations that mimic different reservoir phenomena [25]. Usually, wettability alteration has been considered as a basis for building SWF simulation models [2,21,22,26]. Rock wettability influences the residual saturation of the phases and the relative permeability [17]. Therefore, in most numerical studies, the wettability alteration phenomenon is represented through the water–oil relative permeability curves that are provided as input data for the simulations [2,10,26,27].

These curves are built from the experimental determination of the extreme permeability points for different injected salinity brines and then fit through some model, such as the JBN method, which defines the shape of the curve between these points [27,28]. Different water–oil relative permeability curves are provided, each associated with a wettability state specified by an interpolant parameter. This interpolation criterion correlates the interpolant's current concentration with the system's wettability condition [29]. Different interpolation criteria can also be considered, such as mineral volume fraction, ion concen-

tration in the aqueous phase, or ion-exchange equivalent fraction on the rock surface [30]. During the simulation, this interpolation parameter varies as a function of time and space, and may assume intermediate values between the extremes specified for the provided curves. Therefore, it is necessary to interpolate to obtain the relative permeability value corresponding to this intermediate condition.

Dang (2015) [25] criticizes the use of the total concentration of salts (TDS) as an interpolant because it is not enough to represent the process of smart water flooding. So, using the ion concentration in the aqueous phase is more suitable than TDS for a better numerical adjustment of phenomena in the porous medium. Most works that use this approach adopt the ion equivalent fraction on the rock surface as an interpolant of the relative permeability curves [13,17,31], but without a clear explanation. Specifically for carbonates, the most used interpolant is the SO_4^{2-} or Mg^{2+} equivalent fraction on the rock surface, represented by SO_4-X_2 or Mg-X_2 [3,13,31,32]. But experimentally, it is a complex variable to be quantified because it represents the ions that adhere to the rock surface and not a variable that can be determined from the effluent analysis.

Kadeethum et al. (2017) [33] give an example of a few studies that consider aqueous phase concentration as an interpolant. In this case, Ca^{2+} was the ion selected to mimic a sandstone core's wettability alteration. The authors use the simulator to perform a history-matching of the SWF experiment and then extend the model also to analyze the field scale. In their results, they observed that different combinations of parameters, mainly regarding to relative permeability, can adjust lab simulation results, showing that uncertainties are included in EOR simulations. Interestingly, they indicate that the heterogeneity of the reservoir model is a parameter that influences the values of the interpolant used by them and, consequently, the production estimates obtained. Recently, Moradpour et al. (2020) [34] used sulfate in water as an interpolant in their numerical study of smart water injection into carbonates. However, like most authors, their objective was only to use this interpolant for a historical matching of core flooding experimental results and then a sensitivity analysis of SWF parameters.

Although the selected interpolation criterion usually fits the base case of sensitivity analysis studies from specific experimental conditions and results, there is no assessment of whether other studied scenarios from the variation of parameters of this tuned case are adequately represented. Studies that compare simulations with different interpolants and discuss their influence on the mechanisms have not been identified, as the present study proposes. Kadeethum et al. (2017) [33], assessed the extrapolation of laboratory results to field scale, emphasizing that simulation uncertainties can lead to misleading profit predictions from SWF projects. Therefore, simulation parameters and models must be carefully selected to minimize uncertainties, such as those from the choice of different interpolants.

In this work, a smart water flooding simulation was carried out in a carbonate oil reservoir. The state-of-the-art reports some papers about experimental evaluation of the smart water injection into carbonates and modeling and simulation [2,17,20]. However, little has been found about the relative permeability curves' interpolant influence on SWF simulations since it directly affects the estimation of the recovery curves. It is essential to underline that the relative permeability mimics the effects of wettability alteration. Therefore, the present study differs from the literature because it also considers the gaps in the modeling and simulation of smart water injection into carbonates. The novelty is using an ion concentration in the aqueous phase as an interpolation criterion, different from the ion-exchange equivalent fraction on the rock surface, which has been widely adopted. Furthermore, two other salt ions (Mg^{2+} and SO_4^{2-}) were chosen as criteria for interpolating relative permeability curves to investigate how the interpolant interferes with interpreting the simulated mechanism and, consequently, understanding the true potential of SWF to be applied by oil companies.

For this reason, varying the interpolating factor, this paper proposes to analyze how the wettability alteration is represented and influenced by water salinity and ion composition during SWF in carbonates. This is done by monitoring the oil recovery factor and the

effluent's composition and pH. The interpolant was varied together with the simulation of brines with salinity levels ranging from 30 to 1 kppm and three different water compositions: standard water (STD—with seawater compatible composition), monovalent-rich water (MV), and divalent-rich water (DV).

2. Methodology

In this work, a detailed simulation using a compositional simulator, GEM®, developed by Computer Modeling Group (CMG), investigates smart water core flooding in a carbonate system. The required data and the simulated scenarios are presented as follows.

2.1. Core Flooding Modeling

A carbonate core composed of calcite (50% v/v) and dolomite (50% v/v), 1.5″ diameter and 12″ length, was analyzed in this study. It is a homogeneous and isotropic core whose rock compressibility is 4.0×10^{-6} psi^{-1}, the porosity is 0.2 at any point in the sample, and the permeability is also 200 mD in any direction. The reservoir pressure and temperature conditions used in the core flooding simulation were 1900 psi and 114 °C, respectively. The initial water saturation in the core was set at 0.0894, considering connate water, whose composition is shown in Table 1. Additionally, at 1900 psi and 114 °C, this brine has a density of 68.90 lb/ft^3, a viscosity of 0.469 cP, and a pH 4.9.

Table 1. Connate water composition and properties at reservoir conditions.

Ion	Na^+	K^+	Ca^{2+}	Mg^{2+}	H^+	Cl^-	$SO_4{}^{2-}$	TDS
Concentration (ppm)	54,370	2850	19,740	4070	0.0001	139,800	8	220,838

Live oil was used in this study. Table 2 provides this oil's composition and properties, determined experimentally by Sequeira (2006) [35].

Table 2. Oil composition and properties by Sequeira(2006) [35].

Component	Molar Composition (%)		Component	Molar Composition (%)
CO_2	0.036		N2	0.023
CH_4	23.736		C2H6	0.009
C_3H_8	0.064		NC4	0.342
iC_4	0.117		NC5	0.786
iC_5	0.822		C6	2.644
C_{7+}	71.423			
Molecular weight (g/mol)	164	Gas-oil ratio (ft^3/bbl)	167	Specific Gravity @15 °C	0.8359

Three chemical reactions are required to simulate smart water flooding: aqueous reactions, mineral dissolution/precipitation reactions, and ion-exchange reactions. Considering the presence of CO_2 in the recombined oil, the carbonic acid formation (aqueous reactions) was included in the simulation model, as well as the salts dissolution in the aqueous phase (aqueous reactions) and the mineral dissolution and precipitation reactions of both calcite and dolomite (mineral reactions). Typically, ion exchanges provide the wettability alteration. So, for carbonates, ion sulfate adheres to the rock surface, and the ion exchange reaction should be included in the simulation model (ion exchange reaction). Details of all the reactions involved and the equilibrium constants, as well as models used for phase properties estimates, are provided in Table S1 and Equations (S1)–(S17) of the Supplementary Materials.

The core was modeled using a cartesian geometry divided into 30 equal grids (Figure 1). The injector and production wells were placed in the first and last grid blocks.

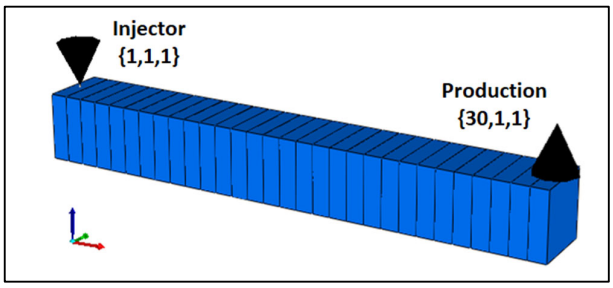

Figure 1. Simulation grid design with Injector well and Production well.

Waterflooding was simulated for an injection flow rate of 0.0006 bbl/day (reservoir condition) during the five days simulated, restricting the maximum pressure at the core inlet to 1950 psi. The pressure at the core outlet was maintained at 1901 psi, establishing a daily production limit of 0.001 barrels of liquid. These conditions were used for all simulated scenarios, described in the next section.

2.2. Simulated Scenarios

Synthetic seawater (STD) was chosen as the base composition of injection water for the core flooding simulation. Brine compositions were prepared by 3-, 6- and 30-times dilutions, named STD3x, STD6x and STD30x, respectively. Two additional brine compositions have also been adopted, departing from STD: one with only monovalent cations—named MV—and the other with divalent cations—named DV. The literature has emphasized the role of divalent cations in the smart water injection process. Some authors have experimentally investigated the use of brines with a variation of these ion concentrations to obtain typical bines rich in specific ions [36,37]. The present work complements the authors' observations through a numerical study, if any of these brines are used. In both cases, MV and DV maintain the total salt concentration of the STD. Similarly, brines diluted 3-, 6- and 30-times were obtained based on MV and DV composition. The ionic concentrations of all brines used in this study are summarized in Table 3.

Table 3. Ionic concentration (in ppm) of the synthetic seawater and smart water evaluated in this study.

	STD	STD 3x	STD 6x	STD 30x	MV	MV 3x	MV 6x	MV 30x	DV	DV 3x	DV 6x	DV 30x
Na^+	11,075	3691.7	1845.8	369.2	11,376	3792.0	1896.0	379.2	0.0	0.0	0.0	0.0
K^+	393	131.0	65.5	13.1	404	134.7	67.3	13.5	0.0	0.0	0.0	0.0
Ca^{2+}	142	47.3	23.7	4.7	0.0	0.0	0.0	0.0	5239	1746.3	873.2	174.6
Mg^{2+}	170	56.7	28.3	5.7	0.0	0.0	0.0	0.0	6541	2180.3	1090.2	218.0
Cl^-	18,847	6282.3	3141.2	628.2	18,847	6282.3	3141.2	628.2	18,847	6282.3	3141.2	628.2
SO_4^{2-}	24	8.0	4.0	0.8	24	8.0	4.0	0.8	24	8.0	4.0	0.8
TDS	30,651	10,217	5108.5	1021.7	30,651	10,217	5108.5	1021.7	30,651	10,217	5108.5	1021.7

By shifting the relative permeability curves, the GEM simulator calculated the wettability alteration to a more water-wet condition. As input data required for simulation, relative permeability data, representing oil wet and water wet conditions from work developed by Dang et al. [38], were used, as shown in Figure 2. The relative permeability curves were built based on information at the endpoints, specifically on the phases' irreducible and critical saturation conditions. The endpoints of the water–oil relative permeability curves change, which is associated with the wettability alteration due to the smart water injection, is also shown in Figure 2. Each curve represents an extreme permeability value associated with the wettability condition: maximum relative oil permeability for water-wet and minimum relative oil permeability for the oil-wet state. The reverse was for relative water permeability of water: minimum permeability for water-wet and maximum permeability for the oil-wet state. In this way, if the concentration of the interpolant ion in a specific grid block during the simulation assumes an intermediate value to these extreme

values represented for set curves, an interpolation is performed to estimate the relative permeability of the water and oil phases, using Equation (1):

$$k_{ri}^{interpolated} = w \cdot k_{ri}^{oil-wet} + (1 - w) \cdot k_{ri}^{water-wet} \quad (1)$$

where: i is the phase water or oil, $k_{ri}{}^{interpolated}$ is the new value of relative permeability calculated by the interpolation for that phase i; $k_{ri}{}^{oil-wet}$ is the value of relative permeability for the phase i, associated with the oil-wet curve presented in Figure 2, $k_{ri}{}^{water-wet}$ is the value of relative permeability for the phase i associated with the water-wet curve shown in Figure 2, and w is an interpolation factor computed by the Equation (2), considering a component aqueous phase concentration as interpolation criterion. Figure 2 shows how the $k_{ro}{}^{oil-wet}$ and $k_{ro}{}^{water-wet}$ values are identified, to calculate the $k_{ro}{}^{interpolated}$ value at point A, whose water saturation is 0.38 and that of oil saturation is 1 − Sw = 0.62.

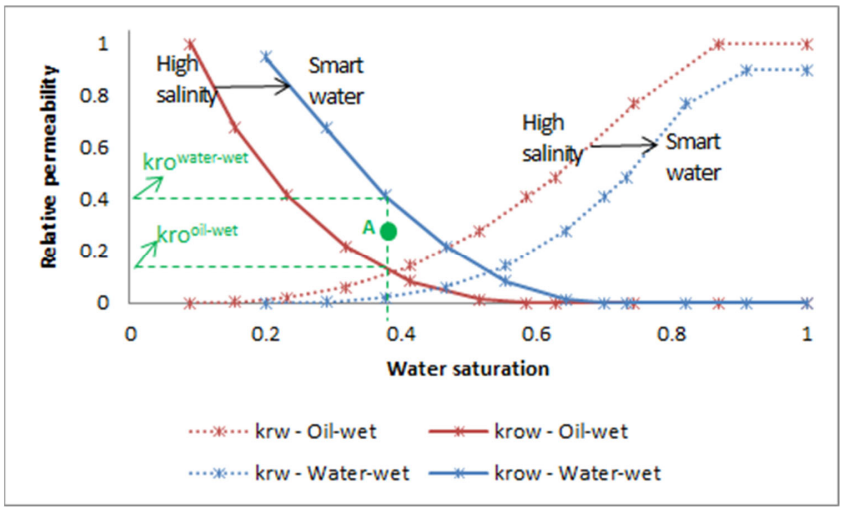

Figure 2. Water–oil relative permeability curves available in Dang et al. [38].

$$w = \left(\frac{x_j^{block,t} - x_j^{oil-wet}}{x_j^{water-wet} - x_j^{oil-wet}} \right)^n \quad (2)$$

where: x is a component aqueous phase concentration, j is related to the interpolant ion used in the specific simulation (Mg^{2+} or $SO_4{}^{2-}$), n is a curvature exponent for the interpolation (defaulted to 1), $x_j{}^{block,t}$ is the ion interpolant concentration calculated in a specific grid block and determined time t during the simulation, $x_j{}^{water-wet}$ is the ion interpolant concentration associated with the water-wet curve set, and $x_j{}^{oil-wet}$ is the ion interpolant concentration associated with the oil-wet curve set.

This study used the interpolation criterion based on the ion concentration in the aqueous phase, specifically $SO_4{}^{2-}$ and Mg^{2+}. Magnesium cation was selected instead of calcium due to the high temperature of the simulated scenario, considering that in this condition, Mg^{2+} has a more critical role than Ca^{2+} [20,23–25]. In this way, 24 different scenarios were investigated, as outlined in Table 4, considering both the variation of the smart water and the interpolation ion.

For the curve corresponding to the oil-wet condition in Figure 2, the concentrations of synthetic seawater were $x_j{}^{oil-wet}$ equal to 24 ppm of $SO_4{}^{2-}$ (when $SO_4{}^{2-}$ is the interpolant ion) and $x_j{}^{oil-wet}$ equal to 170 ppm of Mg^{2+} (when Mg^{2+} is the interpolant ion). And for the curve corresponding to the water-wet condition, concentrations of $x_j{}^{water-wet}$ equal to 0.8 ppm of $SO_4{}^{2-}$ (when $SO_4{}^{2-}$ is the interpolant ion) and $x_j{}^{water-wet}$ equal to 5.7 ppm of Mg^{2+} (when Mg^{2+} is the interpolant ion) were used.

Gas–liquid relative permeability data are shown in Figure S1 of the Supplementary Materials.

Table 4. Overview of all simulated scenarios in this study.

Scenario	Injection Brine	Scenario	Injection Brine	Scenario	Injection Brine	Interpolant Ion
1	STD	9	MV	17	DV	Mg^{2+}
2		10		18		SO_4^{2-}
3	STD 3x	11	MV 3x	19	DV 3x	Mg^{2+}
4		12		20		SO_4^{2-}
5	STD 6x	13	MV 6x	21	DV 6x	Mg^{2+}
6		14		22		SO_4^{2-}
7	STD 30x	15	MV 30x	23	DV 30x	Mg^{2+}
8		16		24		SO_4^{2-}

2.3. Smart Water Mechanisms

An exhaustive discussion is presented in the literature about the role of divalent ions and salinity reduction of injected water in wettability alteration. As highlighted in Figure 3a, carbonate rocks tend to have a positively charged surface, which keeps the negative polar components of the oil adhered and results in initial oil wet behavior that is unfavorable for recovery. Formation water, which has a high concentration of salts, typically has low sulfate content. Through smart water injection, there is a reduction in the total ion concentration in the aqueous phase, which facilitates the access of potential ions to the rock surface. Sulfate is one of these potential ions that must be present in the injected water. Due to its negative charge, it tends to approach the positively charged carbonate and weaken the oil's interactions with the rock in the ion exchange process represented in Figure 3b. Sequentially, other chemical interactions occur between the Ca^{2+} and Mg^{2+} ions and the rock and oil as well as between these ions and the sulfate, exemplified in Figure 3c. In summary, what has been widely accepted is that such interactions and pH increases lead to changes in rock wettability and enhanced recovery [29]. When simulating smart water injection, all these interactions that contribute to the oil recovery mechanism are well represented. As in the simulations, the relative permeability curves fully explain the wettability alteration. The uncertainties arising from the interpolation of these curves can affect this recovery's qualitative and quantitative description. Refining the simulation models, ensuring a good agreement with these phenomena, allows more reliable estimates to support proposals for implementation projects by oil companies.

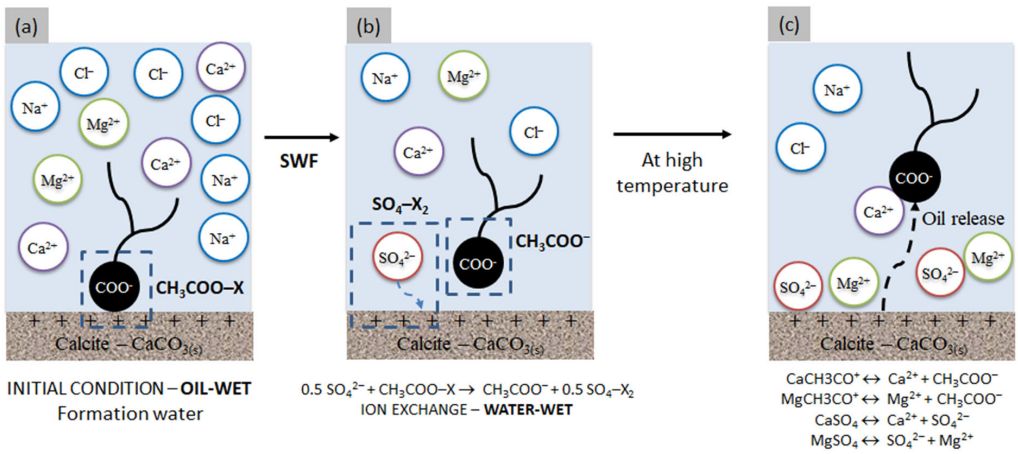

Figure 3. Schematic of smart water injection mechanisms.

3. Results and Discussion

3.1. Oil Behavior Model

PVT experimental data from Sequeira [35] were used for tuning the EOS. This procedure was necessary before the core flooding simulations. The results of the differential liberation experiment data, regressed using the Winprop simulator developed by CMG, are presented in Table S2 and Figures S1–S6 of the Supplementary Materials.

3.2. Core Flooding Simulations

The oil recovery factors obtained for all 24 simulated scenarios are shown in Figure 4. Initially, a quantitative discussion of the results is carried out based on an overview analysis of the influence of salinity reduction and the presence of potential ions on the recovery factor. This work is divided into two sections to present better the results of the core flooding simulations for the different proposed scenarios. The first section discusses the effects of monovalent and divalent cations concentration on oil recovery, as illustrated in Figure 4. The presence of potential ions (Mg^{2+} and SO_4^{2-}) is considered responsible for the wettability alteration, as shown in Figure 3. The second section deals with brine salinity reduction and its effects on SWF. The brine dilution has a more direct relationship with shifting the relative permeability curves intersection to the right, as shown in Figure 2, which physically indicates the wettability alteration from the oil-wet to water-wet state. A comparative discussion of the results obtained depending on the interpolant ion used is presented for both sections. The simulation results and experimental studies at the core scale allow oil recovery estimates, as discussed by Kadeethum et al. (2017) [33]. However, it is imperative to highlight that the extrapolation of these results to the field scale must consider the existing heterogeneity in the reservoirs and the simplifications for carrying out studies on a smaller scale.

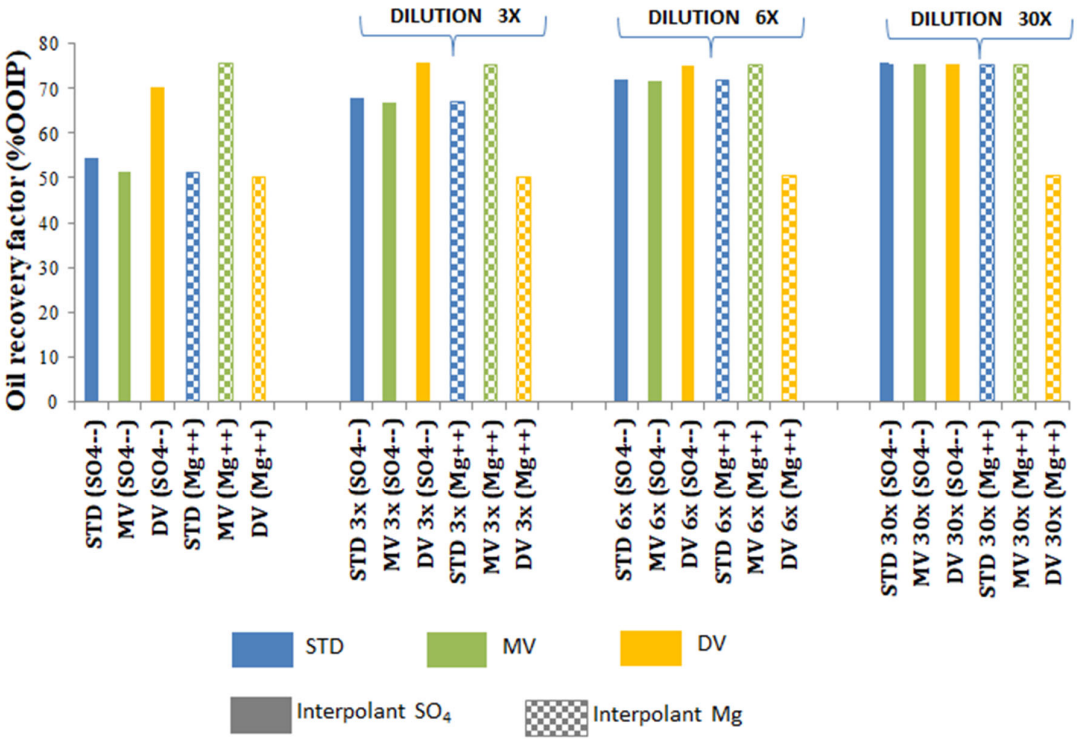

Figure 4. Oil recovery factor versus adopted approach for each simulation.

3.2.1. Monovalent Versus Divalent Cations Effluent Concentration: Influence on Oil Recovery Factor, According to SWF Mechanisms

Oil recovery results for synthetic seawater (STD) flooding compared to those for brines rich in monovalent cations (MV) and brines rich in divalent cations, presented in Figure 4, lead to two distinct trends:

- When sulfate is the interpolant ion, the estimated oil recovery follows a decreasing order: brines rich in divalent cations (DV) > synthetic seawater (STD) > brines rich in monovalent cations (MV). This trend is reversed as long as brine dilutions are evaluated. The recovery is the same for the injection of brine rich in monovalent ions and seawater brine, as seen in the condition of maximum dilution investigated (30x).
- When magnesium is the interpolant ion, the estimated oil recovery occurs in the following order: brines rich in monovalent cations (MV) > synthetic seawater (STD) > brines rich in divalent cations (DV). The recovery factor estimate for injections of synthetic seawater (STD) becomes closer to the results for brines rich in monovalent ions (MV) as the dilution factor increases. For all cases, the recoveries with brines rich in divalent cations (DV) are lower than in the other scenarios.

The reason for these variations and the recovery mechanisms involved can be analyzed through the concentration curves of the interpolating ions in the effluent: SO_4^{2-} shown in Figure 5 and Mg^{2+} in Figure 6, and the interpolation factor w (Equation (2)) variation of the relative permeability curves presented in Figure 7.

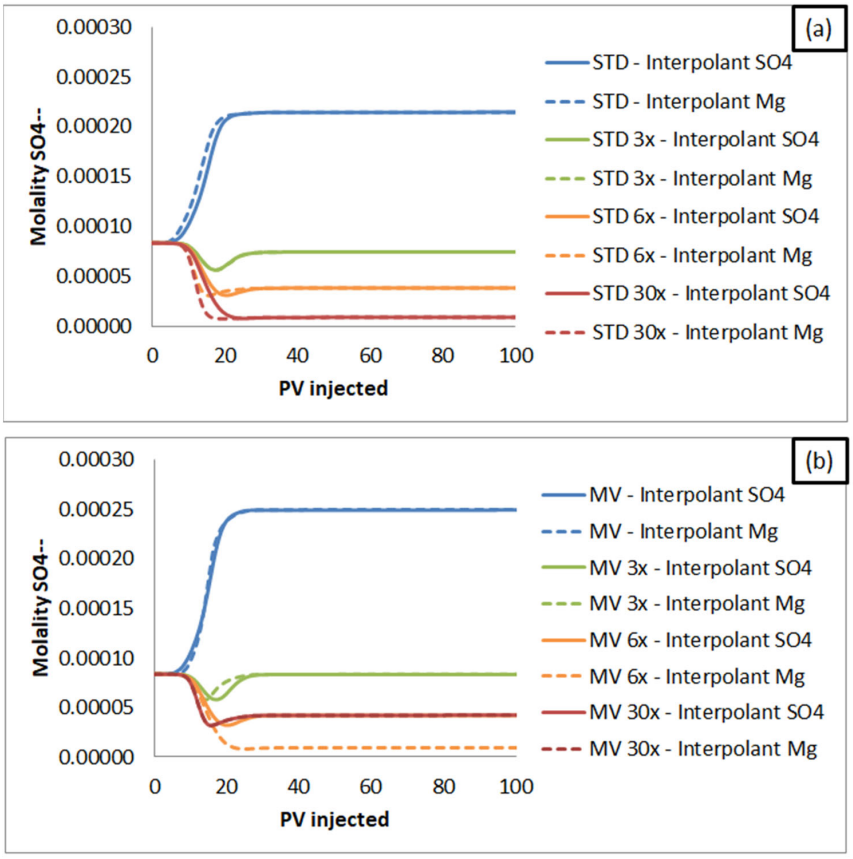

Figure 5. *Cont.*

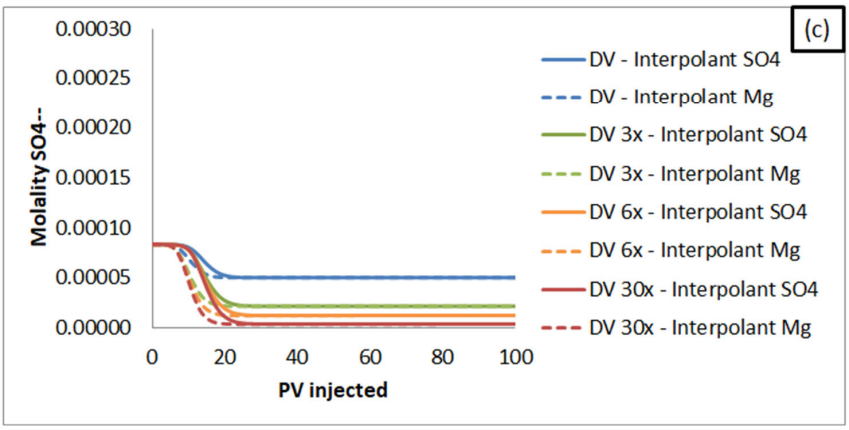

Figure 5. SO_4^{2-} concentration in the effluent for brine injection: (**a**) STD; (**b**) MV and (**c**) DV.

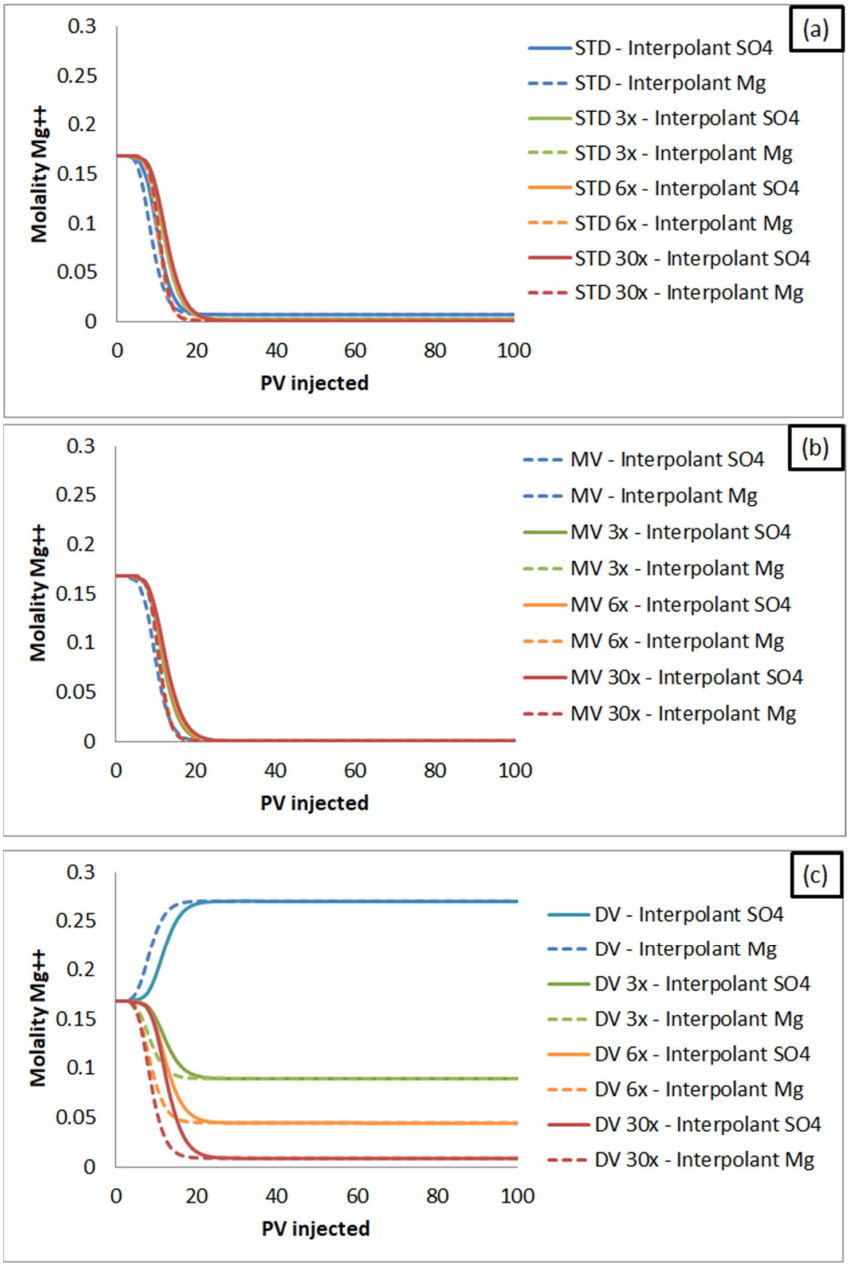

Figure 6. Mg^{2+} concentration in the effluent for brine injection: (**a**) STD; (**b**) MV and (**c**) DV.

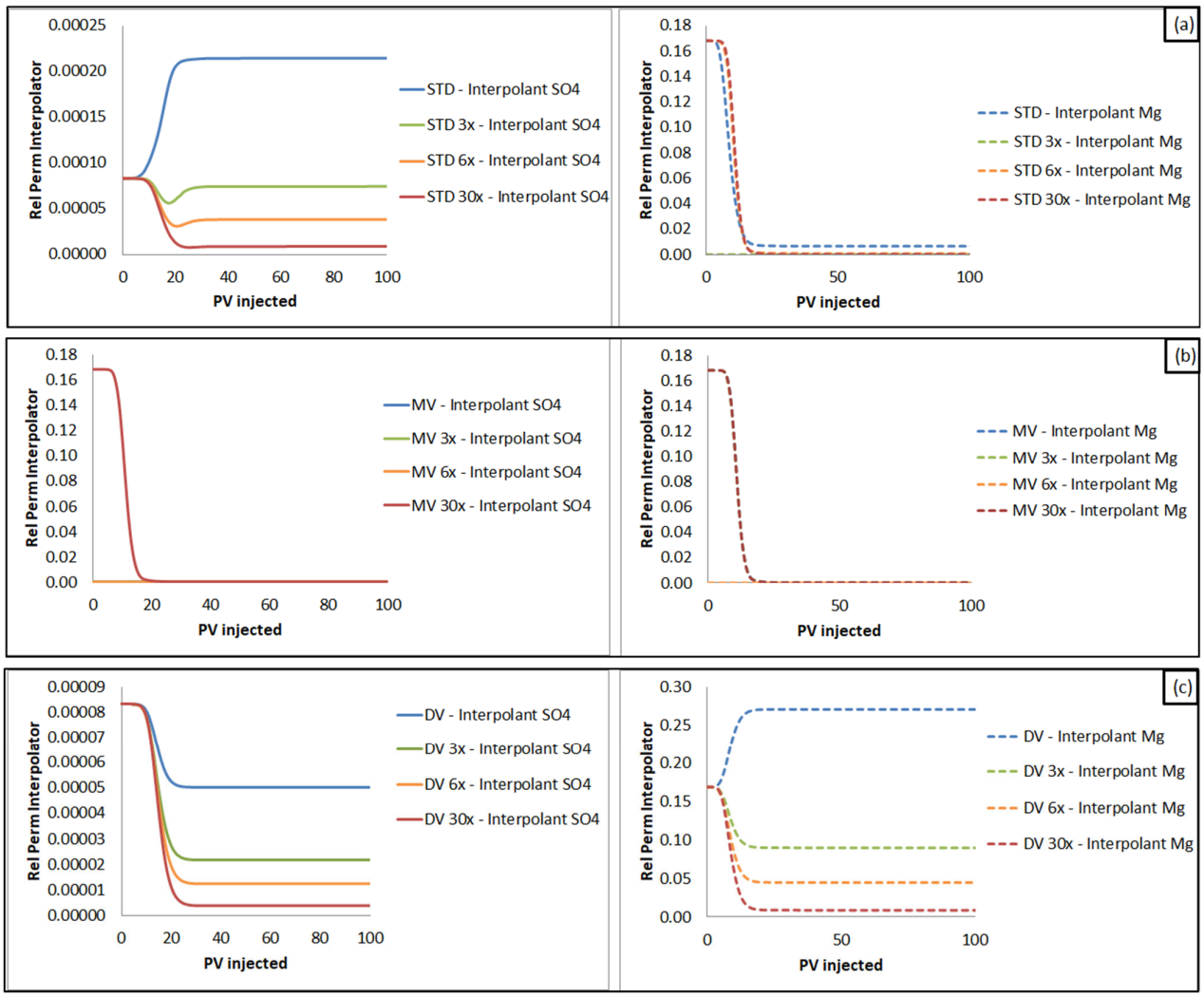

Figure 7. Interpolation factor variation of the relative permeability curves in the grid block {30,1,1} for brine injection: (**a**) STD; (**b**) MV and (**c**) DV.

SO_4^{2-} is a component of all injected brines investigated in this work, as shown in Table 3. Therefore, the variation of this anion concentration was analyzed in the porous medium between the water-wet condition (sulfate molality = 0.000008) and the oil-wet condition (sulfate molality = 0.00025), as represented by point A in the Figure 2. The concentration of SO_4^{2-} in the formation water (initial core condition: sulfate molality = 0.00083) is between these two limit values. The interpolation of the relative permeability curves was performed in this concentration range. It is possible to confirm that the curves with lower sulfate concentration, shown in Figure 5, correspond to the scenarios that showed higher oil recovery factors in Figure 4, since the value of the interpolant tends to approach the curve of the water-wet state.

However, suppose Mg^{2+} is the interpolant ion. In the scenarios with brines rich in monovalent cations, whose magnesium concentration is zero, this ion concentration is considerably reduced, as seen in Figure 6b. Mg^{2+} concentration assumes values near that set for water-wet conditions because magnesium concentration is diluted in the formation water. So, the results are always higher, as they are closer to the most favorable wettability condition for oil recovery. Similar recovery results are also obtained with synthetic seawater and its dilutions because when they are injected, the magnesium concentration is reduced by dilution (Figure 6a), leading to more proximity to the water-wet state (in terms of relative permeability curves). On the other hand, in scenarios with brines rich in divalent cations,

due to the absence of Na^+ and K^+ ions, the magnesium concentration in the medium assumes higher values (Figure 6c) when compared to synthetic seawater. Therefore, the relative permeability for these scenarios is closer to the curve of oil-wet conditions, which leads to lower oil recovery.

Due to the inconsistencies mentioned above, sulfate is the most appropriate ion to be used as an interpolant for the core flooding tests simulated in this work. This anion allows comparison of the effects of divalent and monovalent cations on oil recovery. Based on this conclusion and considering only the results for sulfate as an interpolant, the beneficial effect of increasing Ca^{2+} and Mg^{2+} concentration is evident. Another important observation of these results is that even very low sulfate concentrations, as observed for all simulated injected brines, are highly relevant in the smart water injection process.

Considering Equation 1, the higher the interpolation factor (w), the closer will be the relative permeability to that observed for the oil-wet condition, which results in a lower oil recovery factor. In the oil-wet state, the relative permeability to oil is lower than in the water-wet condition, and, on the other hand, the relative permeability to water is greater than in the water-wet condition. That is, water flow is favored, and oil flow is worse when the curve in Figure 2 is shifted to the left, more oil-wet. For this reason, Figure 7 shows the values of the interpolation factor given by the relative permeability curves. In these cases, w more positive values led to lower recovery estimates, as shown in Figure 4. As the selected interpolant is the concentration of magnesium and sulfate ions in the aqueous phase, the values of the interpolation factor in Figure 7 are directly related to the results shown in Figures 5 and 6.

3.2.2. Dilution Effects: Influence on Oil Recovery Factor, According to SWF Mechanisms

When comparing the results of oil recovery (Figure 4) of concentrated brines (STD, MV and DV) with those of brines with different levels of dilution (3×, 6× and 30×), the main observation was: the more diluted the injected brine, the greater the recovery factor. This recovery improvement with salinity reduction occurred for simulations with synthetic seawater with less abrupt variation in interpolating ion and potential ion concentrations. As seen in Figures 5 and 6, for more dilute injection brines, the interpolant ion concentration is lower, so during the simulation, the relative permeability values are estimated close to those of the relative permeability curve corresponding to the water-wet state (Figure 2), which favors oil recovery. This result reinforces the importance of careful characterization of the relative permeability curves.

These preliminary analyses consider the oil recovery factor estimates as a result of variations in salinity and composition of the injected brines in the range of relative permeability involved. The following discussions, in turn, analyze the pH, effluent concentration and ion exchange equivalent fractions, allowing us to relate the performance obtained with the mechanism involved and represented by the simulator.

3.2.3. Smart Water Flooding Mechanisms Simulation

Additional results were evaluated to ensure the process was captured adequately during the simulations for the different interpolants. From Figures 5 and 6, it is possible to analyze one of the oil recovery mechanisms during the simulation of smart water injection. It was considered that ion exchanges, involving mainly divalent ions, promote a wettability alteration, which, in turn, is represented in the simulations through interpolating the water-oil relative permeability curves. Initially, the aqueous phase is characterized by the composition of the formation water itself. With the injection of the brine of different concentrations and lower total concentrations of salts, two processes coincide and lead to the variation of the interpolant ion concentrations: the dilution and the variation due to ion exchanges. Magnesium has a high concentration in the formation water; with consumption due to exchanges and dilution, its concentration reduces in the effluent. The distinct behavior occurs when the divalent ion-rich brine, which has a significant magnesium concentration, is evaluated so that different levels of Mg^{2+} molality can be seen in the

effluent (Figure 6c). Particularly for a divalent ion-rich brine with 30,000 ppm of total salt concentration (DV), an Mg^{2+} concentration increase is observed. It occurs because the ion exchange losses cannot overcome the continuous injection of brine with a magnesium concentration higher than the formation water. When evaluating the variation of sulfate concentration (Figure 5), the same aspects must be considered. But in this case, the sulfate concentration in the formation water is lower than that of the concentrated brines (STD, MV and DV) and equal to 3× diluted brines (STD 3×, MV 3× and DV 3×). For this sulfate concetration, it is possible to identify an initial concentration reduction as the sum of the dilution and consumption by ion exchange, followed by a concentration increase corresponding to the water breakthrough, i.e., the effluent concentration corresponding to that of the injected water.

Regarding the divalent ion-rich brine (Figure 5c), sulfate concentration in effluent reduces for all dilution scenarios, even for brine with SO_4^{2-} concentration higher than that of formation, for which opposite behavior was expected. In this context, it is essential to highlight that mineral precipitation reactions between Ca^{2+} and Mg^{2+} and sulfate also occur, as indicated in reactions S3 and S4 listed in the Supplementary Materials. The graph in Figure 8 shows the magnesium sulfate precipitation trend in the effluent. As seen in Figure 8c, there is a $MgSO_4$ concentration increase when concentrated DV brine is injected. The discrepancy concerning the trends discussed above may be due to $MgSO_4$ precipitation caused by the high concentration of Mg^{2+} and SO_4^{2-}. It favors the displacement of the reaction $MgSO_4 \leftrightarrow SO_4^{2-} + Mg^{2+}$ to the left side, with additional consumption of sulfate and magnesium ions.

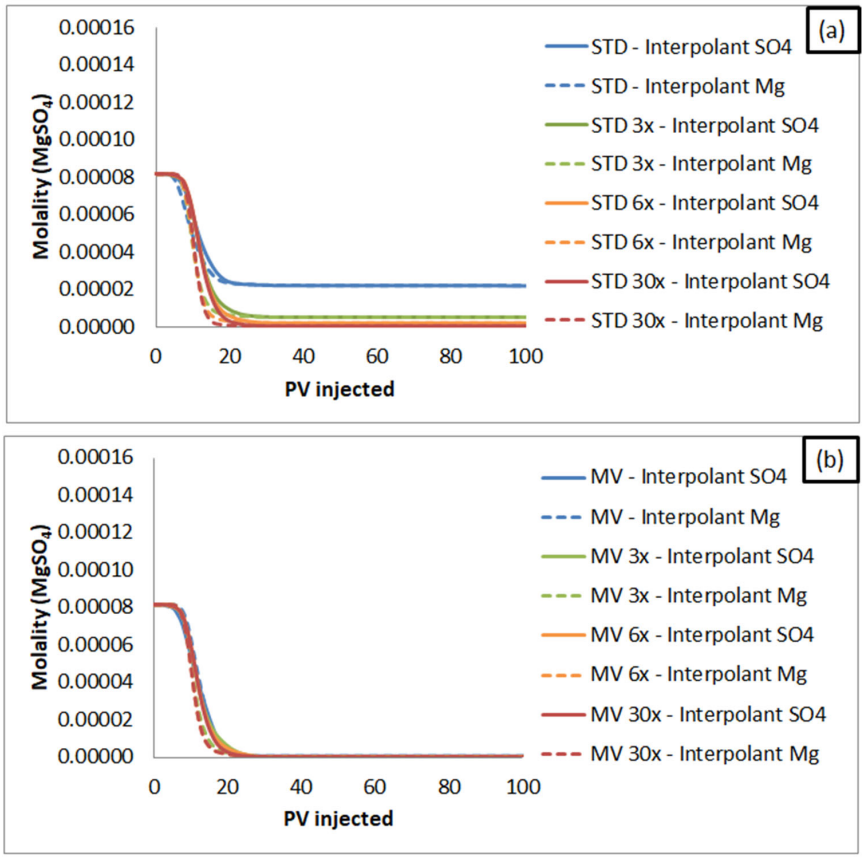

Figure 8. *Cont.*

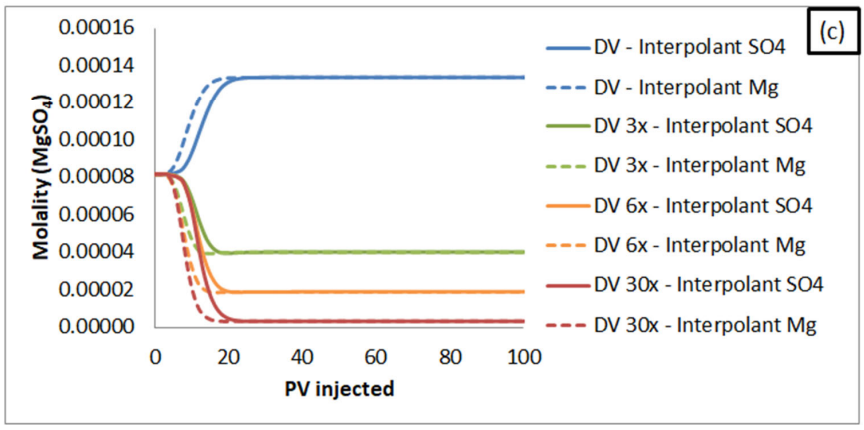

Figure 8. $MgSO_4$ concentration in the effluent for brine injection: (**a**) STD; (**b**) MV and (**c**) DV.

Concerning another physicochemical alteration in the porous medium, Figure 9 shows the pH variation in the effluent as a consequence of the processes that are taking place in the core during smart water injection. Figure 9 shows an increase in the pH of the effluent during the injection for all simulated scenarios, which indicates that the recovery process was adequately described. This increase is also a critical alteration during smart water flooding, observed in most experimental studies. Some authors consider pH one of the main factors leading to wettability alteration [39]. Calcite, one of the main minerals observed in carbonate reservoirs, tends to have a more negative surface charge with pH increase, weakening oil's interaction with rock [12]. This observation was identified mainly based on experimental analyses of zeta potential as a function of pH. But, authors such as Mohammadkhani, Shahverdi and Esfahany (2018) [40] have mentioned that the pH increase is associated with mineral dissolution reactions and cation release but have reinforced that it is not the primary recovery mechanism, mainly when SWF is applied in carbonates.

The evolution of the ion exchange equivalent fractions CH_3COO-X and SO_4-X_2, shown in Figures 10 and 11 respectively, are also important parameters to be examined. The SO_4^{2-} ions adsorb on the minerals during SWF, as schematized in Figure 3, so the SO_4-X_2 equivalent fraction increases. On the other hand, the oil components, represented by CH_3COO^-, are released from the rock. For this reason, the CH_3COO-X equivalent fraction decreases. The monitoring of the CH_3COO-X equivalent fraction, shown in Figure 10, represents the inverse of the recovery factor since the smaller the oil fraction still adhered to the rock, the greater the amount of oil that was produced. Therefore, this fraction indicates, from a complementary point of view, how the simulator evaluates the recovery mechanism. Analogously, the SO_4-X_2 equivalent fraction represents the mechanism precursor, initiating the ion exchange, as shown in Figure 3.

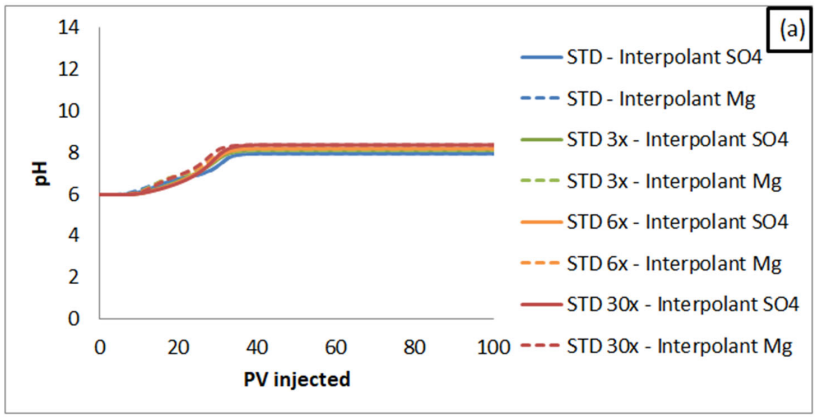

Figure 9. *Cont.*

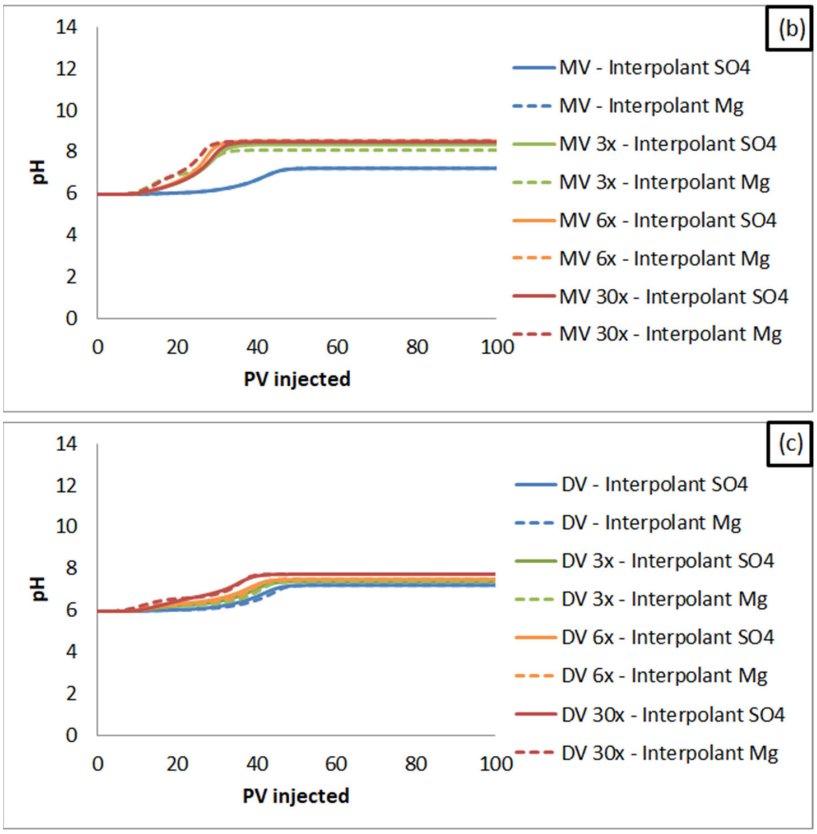

Figure 9. pH of the effluent for brine injection: (**a**) STD; (**b**) MV and (**c**) DV.

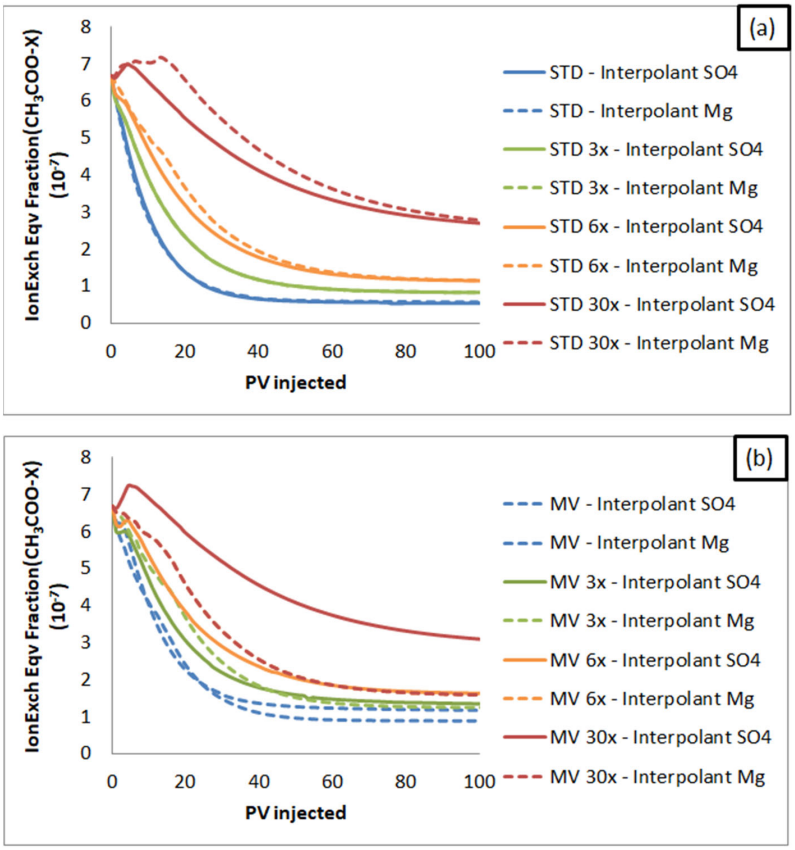

Figure 10. *Cont.*

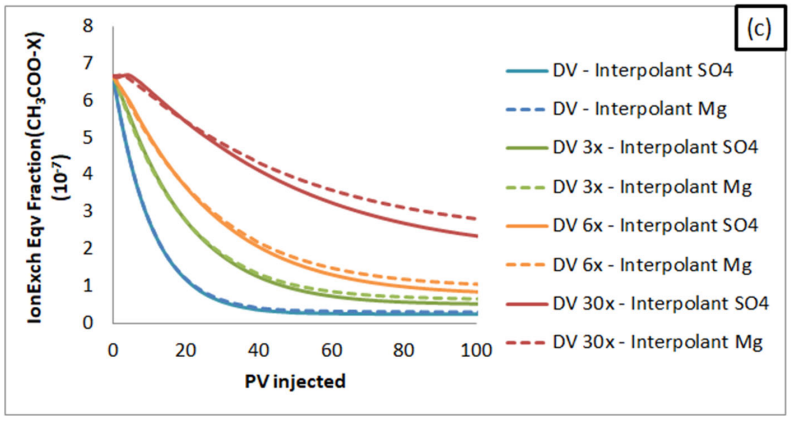

Figure 10. Ion Exchange Equivalent Fraction (CH_3COO-X) variation in the grid block {1,1,1} for brine injection: (**a**) STD; (**b**) MV and (**c**) DV.

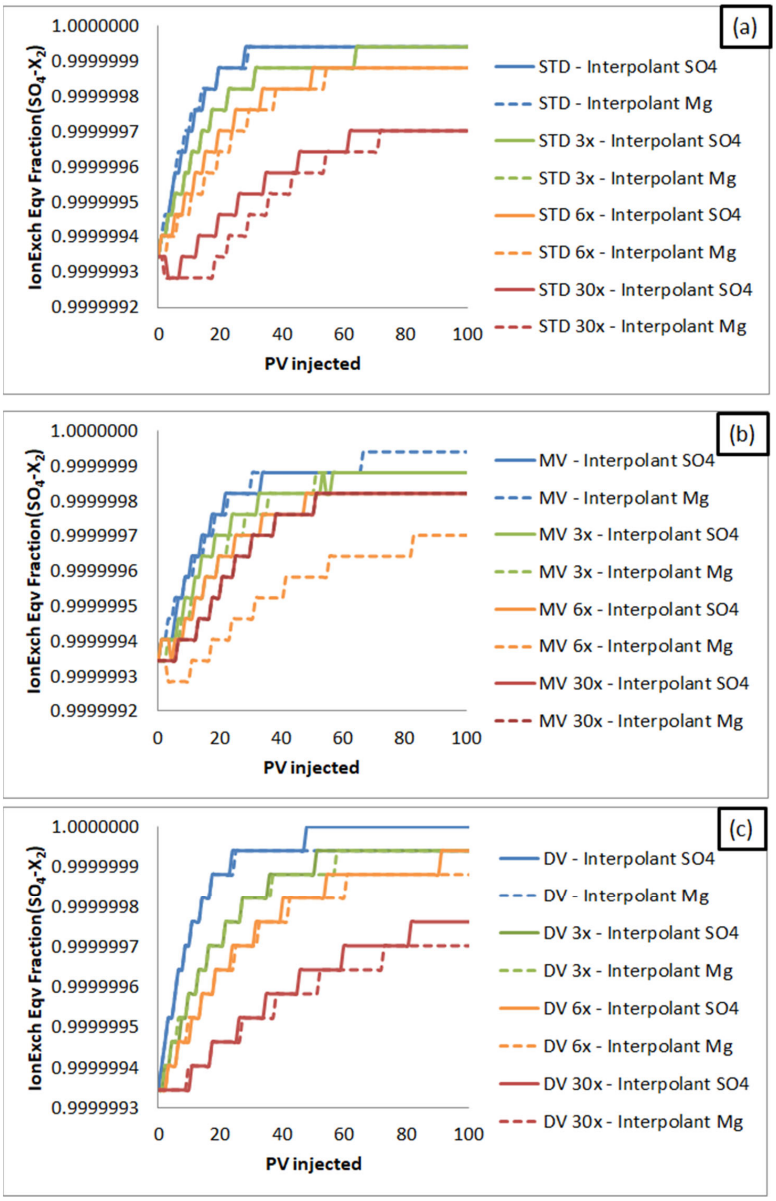

Figure 11. Ion Exchange Equivalent Fraction (SO_4-X_2) variation in the grid block {1,1,1} for brine injection: (**a**) STD; (**b**) MV and (**c**) DV.

4. Conclusions

The wettability alteration is the most accepted effect to explain improved recovery through smart water injection. In simulators, this phenomenon is represented through the shifting of water–oil relative permeability curves. This paper provides a detailed simulation study investigating smart water flooding in a carbonate system. The effects of water salinity and ion composition on oil recovery are described. The primary purpose was to evaluate the impact that the selection of different interpolants has on the representation of mechanisms related to SWF and the oil recovery estimates. In the literature, the interpolant is typically used only for historic matching, and no studies have been observed that deal with their use to assess mechanisms. In this work, Mg^{2+} and $SO_4{}^{2-}$ concentrations in the aqueous phase were used as interpolant ions of relative permeability curves. The simulation results demonstrated the significant influence of the interpolant on oil recovery estimates. For each interpolant, RF also changes significantly as a function of salinity and composition. The greater the dilution, the smaller the influence of the interpolant and brine composition on the recovery estimates. When considering $SO_4{}^{2-}$ as an interpolant, the trend is that the divalent rich brine (DV) has a higher recovery factor. In contrast, when Mg^{2+} is the interpolant, DV tends to have a lower recovery. Both interpolants have reproduced the pH increase and ion exchange mechanisms associated with carbonate wettability alteration well. This behavior has been observed through geochemical analysis from effluent composition in the scenarios studied. Results based on the alteration of carbonate wettability also support the beneficial effect of divalent ions and salinity reduction on oil recovery. Future works will include the experimental validation of the observed results.

Supplementary Materials: The following supporting information can be downloaded at: https://www.mdpi.com/article/10.3390/en16010446/s1, Figure S1: Gas-Oil relative permeability curve; Figure S2: Data regression of differential liberation experiment—Gas-oil ratio; Figure S3: Data regression of differential liberation experiment—Oil specific gravity; Figure S4: Data regression of differential liberation experiment—Gas specific gravity; Figure S5: Data regression of differential liberation experiment—Oil viscosity; Figure S6: Data regression of constant composition expansion experiment—Oil density; Table S1: Modeling of phase properties in the GEM simulator; Table S2: Average deviation of the properties estimated by the model after regression of the PVT data. References [41–44] have been cited in the supplementary material.

Author Contributions: L.d.S.B.: Conceptualization, Methodology, Investigation, Writing—original draft preparation, Writing—review and editing; I.E.d.S.L.: Conceptualization, Methodology, Investigation, Writing—original draft preparation, Writing—review and editing; G.M.N.C.: Conceptualization, Methodology, Investigation, Writing—original draft preparation, Writing—review and editing, Supervision, and Project administration; S.A.B.V.d.M.: Conceptualization, Writing—review and editing, Supervision, Project administration, and Funding acquisition. All authors have read and agreed to the published version of the manuscript.

Funding: This research was funded by Petrogal Brasil S.A., grant number 20623-5.

Data Availability Statement: Not applicable.

Acknowledgments: The authors acknowledge the Agência Nacional de Petróleo, Gás Natural e Biocombustíveis (ANP) and the Petrogal Brasil S.A., related to the grant from the R&D rule, as well as the CMG's Engineer Juan Mateo.

Conflicts of Interest: The authors declare no conflict of interest.

References

1. Rahimi, A.; Honarvar, B.; Safari, M. The Role of Salinity and Aging Time on Carbonate Reservoir in Low Salinity Seawater and Smart Seawater Flooding. *J. Pet. Sci. Eng.* **2020**, *187*, 106739. [CrossRef]
2. Sohal, M.A.; Thyne, G.; Søgaard, E.G. Review of Recovery Mechanisms of Ionically Modified Waterflood in Carbonate Reservoirs. *Energy Fuels* **2016**, *30*, 1904–1914. [CrossRef]
3. Egbe, D.I.O.; Jahanbani Ghahfarokhi, A.; Nait Amar, M.; Torsæter, O. Application of Low-Salinity Waterflooding in Carbonate Cores: A Geochemical Modeling Study. *Nat. Resour. Res.* **2021**, *30*, 519–542. [CrossRef]

4. Xu, Z.X.; Li, S.Y.; Li, B.F.; Chen, D.Q.; Liu, Z.Y.; Li, Z.M. A Review of Development Methods and EOR Technologies for Carbonate Reservoirs. *Pet. Sci.* **2020**, *17*, 990–1013. [CrossRef]
5. Al-Shalabi, E.W.; Sepehrnoori, K.; Pope, G. Geochemical Interpretation of Low-Salinity-Water Injection in Carbonate Oil Reservoirs. *SPE J.* **2015**, *20*, 1212–1226. [CrossRef]
6. Zallaghi, M.; Khaz'ali, A.R. Experimental and Modeling Study of Enhanced Oil Recovery from Carbonate Reservoirs with Smart Water and Surfactant Injection. *Fuel* **2021**, *304*, 121516. [CrossRef]
7. Lashkarbolooki, M.; Ayatollahi, S.; Riazi, M. Mechanistical Study of Effect of Ions in Smart Water Injection into Carbonate Oil Reservoir. *Process. Saf. Environ. Prot.* **2017**, *105*, 361–372. [CrossRef]
8. Yousef, A.A.; Al-Saleh, S.; Al-Jawfi, M. New Recovery Method for Carbonate Reservoirs through Tuning the Injection Water Salinity: Smart WaterFlooding. In Proceedings of the SPE EUROPEC/EAGE Annual Conference and Exhibition, Vienna, Austria, 23–26 May 2011.
9. Yousef, A.A.; Al-Saleh, S.; Al-Jawfi, M. Smart Waterflooding for Carbonate Reservoirs: Salinity and Role of Ions. *SPE Middle East Oil Gas Show Conf. MEOS Proc.* **2011**, *1*, 632–642. [CrossRef]
10. Yousef, A.A.; Liu, J.; Blanchard, G.; Al-Saleh, S.; Al-Zahrani, T.; Al-Zahrani, R.; Al-Tammar, H.; Al-Mulhim, N. SmartWater Flooding: Industry's First Field Test in Carbonate Reservoirs. In Proceedings of the SPE Annual Technical Conference and Exhibition, San Antonio, Texas, USA, 8–10 October 2012.
11. Rassenfoss, S. Scaling Up Smart Water. *J. Pet. Technol.* **2016**, *68*, 39–41. [CrossRef]
12. Hao, J.; Mohammadkhani, S.; Shahverdi, H.; Esfahany, M.N.; Shapiro, A. Mechanisms of Smart Waterflooding in Carbonate Oil Reservoirs—A Review. *J. Pet. Sci. Eng.* **2019**, *179*, 276–291. [CrossRef]
13. Elgendy, A.M.S.; Porta, G.M. Impact of Reservoir Geochemistry on Low Salinity Waterflooding: Global Sensitivity Analysis. *J. Pet. Sci. Eng.* **2021**, *207*, 109056. [CrossRef]
14. Zhang, T.; Li, Y.; Li, C.; Sun, S. Effect of Salinity on Oil Production: Review on Low Salinity Waterflooding Mechanisms and Exploratory Study on Pipeline Scaling. *Oil Gas Sci. Technol.* **2020**, *75*, 50. [CrossRef]
15. Mahmoudpour, M.; Pourafshary, P. Investigation of the Effect of Engineered Water/Nanofluid Hybrid Injection on Enhanced Oil Recovery Mechanisms in Carbonate Reservoirs. *J. Pet. Sci. Eng.* **2021**, *196*, 107662. [CrossRef]
16. Al Shalabi, E.W.; Sepehrnoori, K.; Delshad, M. Mechanisms behind Low Salinity Water Injection in Carbonate Reservoirs. *Fuel* **2014**, *121*, 11–19. [CrossRef]
17. Awolayo, A.N.; Sarma, H.K.; Nghiem, L.X. A Comprehensive Geochemical-Based Approach at Modeling and Interpreting Brine Dilution in Carbonate Reservoirs. In Proceedings of the SPE Reservoir Simulation Conference 2017, Montgomery, TX, USA, 20–22 February 2017; pp. 648–674. [CrossRef]
18. Strand, S.; Puntervold, T. Recent Updates on Smart Water EOR in Limestone. In Proceedings of the Offshore Technology Conference Brasil, Rio de Janeiro, Brazil, 29–31 October 2019; pp. 29–31. [CrossRef]
19. Shapoval, A.; Haryono, D.; Cao, J.L.; Rahman, S.S. Pore-Scale Investigation of the Ion-Tuned Water Effect on the Surface Properties of Limestone Reservoirs. *Energy Fuels* **2021**, *35*, 10475–10487. [CrossRef]
20. Rezaeidoust, A.; Puntervold, T.; Strand, S.; Austad, T. Smart Water as Wettability Modifier in Carbonate and Sandstone: A Discussion of Similarities/Differences in the Chemical Mechanisms. *Energy Fuels* **2009**, *23*, 4479–4485. [CrossRef]
21. Al-Shalabi, E.W.; Sepehrnoori, K.; Delshad, M.; Pope, G. A Novel Method to Model Low-Salinity-Water Injection in Carbonate Oil Reservoirs. *SPE J.* **2015**, *20*, 1154–1166. [CrossRef]
22. Nande, S.B.; Patwardhan, S.D. A Review on Low Salinity Waterflooding in Carbonates: Challenges and Future Perspective. *J. Pet. Explor. Prod. Technol.* **2022**, *12*, 1037–1055. [CrossRef]
23. Fathi, S.J.; Austad, T.; Strand, S. Water-Based Enhanced Oil Recovery (EOR) by "Smart Water" in Carbonate Reservoirs. In Proceedings of the SPE EOR Conference at Oil and Gas West Asia, Muscat, Oman, 16–18 April 2012; Volume 1, pp. 349–362. [CrossRef]
24. Moradpour, N.; Pourafshary, P.; Zivar, D. Experimental Analysis of Hybrid Low Salinity Water Alternating Gas Injection and the Underlying Mechanisms in Carbonates. *J. Pet. Sci. Eng.* **2021**, *202*, 108562. [CrossRef]
25. Dang, C.T.Q. Mechanistic Modeling of Low Salinity Waterflooding: Flow and Transport Model. Ph.D. Thesis, University of Calgary, Calgary, AB, Canada, 2015; p. 324. [CrossRef]
26. Alshakhs, M.J.; BuKhamseen, N.Y.; AlGarni, S.A. Paradigm Shift in Smartwater Simulation Methods. In Proceedings of the International Petroleum Technology Conference 2020, Dhahran, Saudi Arabia, 13–15 January 2020; pp. 13–15. [CrossRef]
27. Dang, C.; Nghiem, L.; Nguyen, N.; Chen, Z.; Nguyen, Q. Modeling and Optimization of Low Salinity Waterflood. In Proceedings of the SPE Reservoir Simulation Symposium, Houston, TX, USA, 23–25 February 2015; pp. 1–19. [CrossRef]
28. Al-Shalabi, E.W.; Sepehrnoori, K.; Pope, G. Mysteries behind the Low Salinity Water Injection Technique. *J. Pet. Eng.* **2014**, *2014*, 304312. [CrossRef]
29. Nguyen, N.; Dang, C.; Gorucu, S.E.; Nghiem, L.; Chen, Z. The Role of Fines Transport in Low Salinity Waterflooding and Hybrid Recovery Processes. *Fuel* **2020**, *263*, 116542. [CrossRef]
30. Gorucu, S.E.; Dang, C.; Nghiem, L.; Shrivastava, V. Modeling and Optimization of Low Salinity Waterflood with Fines Transport. In Proceedings of the SPE Annual Technical Conference and Exhibition, Calgary, AB, Canada, 30 September–2 October 2019. [CrossRef]

31. Esene, C.; Onalo, D.; Zendehboudi, S.; James, L.; Aborig, A.; Butt, S. Modeling Investigation of Low Salinity Water Injection in Sandstones and Carbonates: Effect of Na+ and SO42−. *Fuel* **2018**, *232*, 362–373. [CrossRef]
32. Adegbite, J.O.; Al-Shalabi, E.W.; Ghosh, B. Geochemical Modeling of Engineered Water Injection Effect on Oil Recovery from Carbonate Cores. *J. Pet. Sci. Eng.* **2018**, *170*, 696–711. [CrossRef]
33. Kadeethum, T.; Sarma, H.K.; Maini, B.B.; Jaruwattanasakul, C. Uncertainties–Extension of Smart Waterflooding from Core to Field Scale. In Proceedings of the IOR 2017—19th European Symposium on Improved Oil Recovery, Stavanger, Norway, 24–27 April 2017. [CrossRef]
34. Moradpour, N.; Karimova, M.; Pourafshary, P.; Zivar, D. Effects of Slug Size, Soaking, and Injection Schemes on the Performance of Controlled Ions Water Flooding in Carbonates. *ACS Omega* **2020**, *5*, 18155–18167. [CrossRef]
35. Sequeira, D.S. Compositional Effects on Gas-Oil Interfacial Tension and Miscibility at Reservoir Conditions. Master's Thesis, Louisiana State University, Baton Rouge, LA, USA, 2006.
36. Purswani, P.; Karpyn, Z.T. Laboratory Investigation of Chemical Mechanisms Driving Oil Recovery from Oil-Wet Carbonate Rocks. *Fuel* **2019**, *235*, 406–415. [CrossRef]
37. Sarvestani, A.D.; Ayatollahi, S.; Bahari Moghaddam, M. Smart Water Flooding Performance in Carbonate Reservoirs: An Experimental Approach for Tertiary Oil Recovery. *J. Pet. Explor. Prod. Technol.* **2019**, *9*, 2643–2657. [CrossRef]
38. Dang, C.T.Q.; Nghiem, L.X.; Chen, Z.; Nguyen, N.T.B.; Nguyen, Q.P. CO2 Low Salinity Water Alternating Gas: A New Promising Approach for Enhanced Oil Recovery. In Proceedings of the SPE Improved Oil Recovery Symposium, Tulsa, OK, USA, 12–16 April 2014; Volume 1, pp. 578–596.
39. Sagbana, I.P.; Sarkodie, K.; Nkrumah, W.A. A Critical Review of Carbonate Reservoir Wettability Modi Fi Cation during Low Salinity Water Flooding. *Petroleum* **2022**, *in press*. [CrossRef]
40. Mohammadkhani, S.; Shahverdi, H.; Esfahany, M.N. Impact of Salinity and Connate Water on Low Salinity Water Injection in Secondary and Tertiary Stages for Enhanced Oil Recovery in Carbonate Oil Reservoirs. *J. Geophys. Eng.* **2018**, *15*, 1242–1254. [CrossRef]
41. Peng, D.Y.; Robinson, D.B. A New Two-Constant Equation of State. *Ind. Eng. Chem. Fundam.* **1976**, *15*, 59–64. [CrossRef]
42. Jossi, J.A.; Stiel, L.I.; Thodos, G. The Viscosity of Pure Substances in the Dense Gaseous and Liquid Phases. *AIChE J.* **1962**, *8*, 59–63. [CrossRef]
43. Yoonm, P.; Thodos, G. Viscosity of Nonpolar Gaseous Mixtures at Normal Pressures. *AIChE J.* **1970**, *16*, 300–304. [CrossRef]
44. Kestin, J.; Khalifa, H.E.; Sookiazian, H.; Wakeham, W.A. Experimental Investigation of Pressure Effect on the Viscosity of Water in the Temperature Range 10–15 °C. *Ber. Bunsenges./Phys. Chem. Chem. Phys.* **1978**, *82*, 180–188. [CrossRef]

Disclaimer/Publisher's Note: The statements, opinions and data contained in all publications are solely those of the individual author(s) and contributor(s) and not of MDPI and/or the editor(s). MDPI and/or the editor(s) disclaim responsibility for any injury to people or property resulting from any ideas, methods, instructions or products referred to in the content.